Letter

Interaction-mitigated Landau damping

Xuepeng Wang,[1] Roderich Moessner,[2] and Debanjan Chowdhury[1]
[1]*Department of Physics, Cornell University, Ithaca, New York 14853, USA*
[2]*Max-Planck-Institut für Physik komplexer Systeme, Nöthnitzer Straße 38, 01187 Dresden, Germany*

(Received 8 August 2023; revised 16 January 2024; accepted 13 February 2024; published 6 March 2024)

Bosonic collective modes are ubiquitous in metals, but over a wide range of energy and momenta suffer from Landau damping, decaying into the continuum of particle-hole excitations. Here we point out that interactions can suppress this decay, protecting a finite fraction of the total spectral weight associated with the collective mode, e.g., a plasmon. The underlying mechanism is level repulsion between a discrete mode and the continuum. We demonstrate the effect using a number of simplified models of strongly correlated Fermi-liquid metals, including a solvable random flavor model in the large-N limit. We discuss in detail the possibility of observing such an avoided decay for plasmons in (moiré) graphenelike systems.

DOI: 10.1103/PhysRevB.109.L121102

Introduction. Weakly interacting Fermi-liquid (FL) metals have a qualitatively universal excitation spectrum [1]. In the vicinity of the sharply defined Fermi surface, single-particle excitations correspond to the long-lived renormalized quasiparticles. The two-particle excitations associated with the density fluctuations in a neutral FL include: (i) the particle-hole (ph) continuum, which contains significant spectral weight over a range of frequencies, $0 \leqslant \omega \lesssim W(\equiv \text{bandwidth})$, and momenta, $0 \leqslant q \leqslant 2k_F$ ($k_F \equiv$ Fermi momentum), and (ii) a gapless collective (zero-sound) mode associated with fluctuations of the entire Fermi surface [2]. In a charged FL where electrons interact via Coulomb interactions, the zero-sound mode renormalizes into the plasmon excitation, which can either be gapless or gapped depending on the interplay of dimensionality and screening. The spectral weight in the ph continuum has a sharp onset across a dispersive threshold, $\omega_\star(\boldsymbol{q})$; the collective modes in a FL generically enter the ph continuum at sufficiently large $\boldsymbol{q}$ and acquire a finite lifetime, decaying via Landau damping. Finding routes to avoid this (kinematically seemingly inevitable) decay of collective modes into the continuum has important experimental and technological implications. For instance, one of the main challenges in the field of plasmonics is tied to the plasmon decay [3,4].

Here, we demonstrate, by a combination of analytics for solvable models and explicit numerics, that a collective mode in an interacting metal can avoid disappearing into the ph continuum. Instead the continuum partially repels it, placing a finite amount of its spectral weight outside and thereby partially eliminating Landau damping.

We explicitly demonstrate this effect using examples of well-known materials, such as (moiré) graphene. While the parameter regimes required to display level repulsion for these materials in an experimentally resolvable fashion might lie outside current capabilities, it seems eminently possible that there exist closely related materials where the effect can be probed directly in the not too distant future. The basic mechanism for such a kinematically allowed [5,6] but avoided decay was identified [7] when it was noted that a quasiparticle (e.g., magnon) could be repelled by its own two-particle continuum, with repulsion between a discrete level and a continuum studied in Ref. [8]. The present work extends this to the setting of metals, where an abundance of gapless excitations tied to the metallic Fermi surface leads to a continuum that persists down to $\omega \to 0$, which necessitates a careful analysis of the fate of the collective modes. In addition, the plasmon can exhibit an interaction-derived gap, which distinguishes it from Goldstone modes in magnetic systems.

Model. A simple low-energy theory that illustrates the mechanism of level repulsion of a gapped bosonic collective mode from the ph continuum associated with a Fermi liquid metal has the following Matsubara action:

$$S[c^\dagger, c, \Phi] = S_c + S_\Phi + S_{\text{int}}, \tag{1a}$$

$$S_c = \sum_k c_k^\dagger (i\omega_n - \varepsilon_{\boldsymbol{k}}) c_k, \tag{1b}$$

$$S_\Phi = \sum_q \left(\Omega_n^2 + \rho_s \boldsymbol{q}^2 + \Delta^2\right) |\Phi_q|^2, \tag{1c}$$

$$S_{\text{int}} = \lambda \sum_{k,q} \Phi_q c_{k+q}^\dagger c_k. \tag{1d}$$

The fields $c_k^\dagger$, c_k denote the electronic quasiparticle creation and annihilation operators with dispersion $\varepsilon_{\boldsymbol{k}}$. The bosonic collective mode, Φ, has a gap Δ, and stiffness ρ_s. It is coupled to a ph excitation via a Yukawa coupling of strength, λ. We use a shorthand notation, $k \equiv (i\omega_n, \boldsymbol{k})$ and $q \equiv (i\Omega_n, \boldsymbol{q})$, where $i\omega_n$ ($i\Omega_n$) represent fermionic (bosonic) Matsubara frequencies, respectively.

Analytical results. For analytic tractability, we linearize the dispersion near the Fermi surface, $\varepsilon_{\boldsymbol{k}} \approx v_c |\delta \boldsymbol{k}|$, where $|\delta \boldsymbol{k}|$ measures the deviation around the Fermi momentum. Tracing out the c electrons yields an effective theory purely in terms of the collective modes:

$$S_{\text{eff}}[\Phi] = \sum_q [\Omega^2 - (\rho_s \boldsymbol{q}^2 + \Delta^2) + \Pi_c(\boldsymbol{q}, \Omega)] \Phi_q \Phi_{-q}, \tag{2a}$$

$$\Pi_c(\boldsymbol{q}, \Omega) = \frac{\lambda^2}{v_c} \left[1 - \frac{\Omega}{\sqrt{\Omega^2 - (v_c \boldsymbol{q})^2}}\right]. \tag{2b}$$

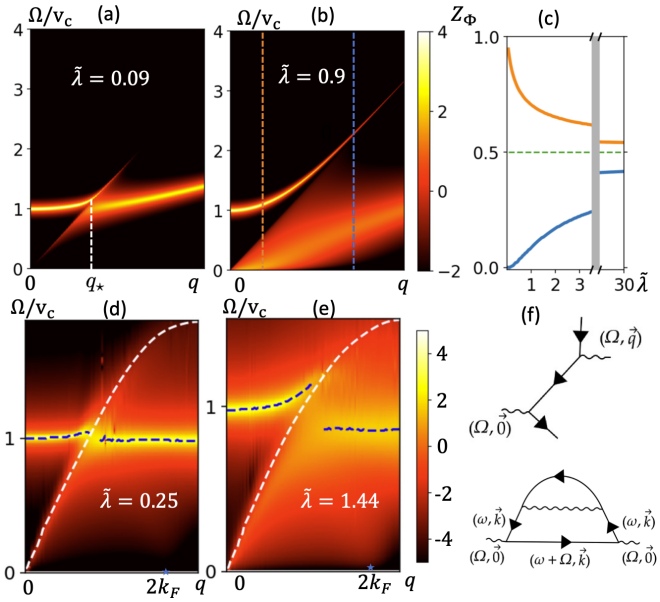

FIG. 1. The response function $\log[\mathrm{Im}D(\boldsymbol{q},\Omega)]$ in Eq. (3) obtained from Eq. (1), evaluated at (a) weak ($\tilde{\lambda}=0.09$) and (b) strong ($\tilde{\lambda}=0.9$) coupling, respectively. We introduce a small broadening, $\eta=0.01$, for visualization purpose when evaluating $\mathrm{Im}D(\boldsymbol{q},\Omega+i\eta)$. The white vertical dashed line in (a) labels the momentum q_* at which the collective mode crosses the onset of the ph continuum when $\lambda=0$. (c) Numerically obtained Z_Φ as a function of $\tilde{\lambda}$ for two different q values [vertical colored dashed lines in (b)]. We set $\widetilde{\Delta}=0.5$ to be in the regime where the asymptotic limit in Eq. (5a) is justified. (d)–(e) Disorder-averaged results for $\log[\mathrm{Im}D(\boldsymbol{q},\Omega)]$ for the random flavor model with $t_c=1$, $\Delta=1$, $\mu=-1.25t_c$ and interaction strengths (d) $\lambda=0.5$, and (e) $\lambda=1.2$, respectively. The corresponding $\tilde{\lambda}$ is defined as described in the main text. White dashed lines denote the onset of the continuum. Blue dashed lines denote the peak associated with $\mathrm{Im}[D(\boldsymbol{q},\Omega)]$, corresponding to the renormalized collective mode. The electronic quasiparticle residue, Z_c, is obtained self-consistently by solving the saddle point equation [9], with (d) $Z_c\sim 0.9$, and (e) $Z_c\sim 0.8$, respectively. (f) Feynman diagrams for multiparticle scattering processes and the leading-order self-energy for the collective mode.

We introduce dimensionless units, $\tilde{\lambda}=\lambda^2/v_c^3$, $\widetilde{\Omega}=\Omega/v_c$, $\widetilde{\rho}_s=\rho_s/v_c^2$, and $\widetilde{\Delta}=\Delta/v_c$. We set the lattice constant $a=1$ for convenience; so that $\boldsymbol{q}$ denotes a dimensionless momentum. Henceforth we focus specifically on two-dimensional systems; the approach can be similarly extended to higher dimensions in an analogous fashion. The renormalized Φ propagator can then be expressed as

$$D(\boldsymbol{q},\Omega)=\frac{1/v_c^2}{\left[\widetilde{\Omega}^2-(\widetilde{\rho}_s\boldsymbol{q}^2+\widetilde{\Delta}^2-\tilde{\lambda})-\frac{\tilde{\lambda}\widetilde{\Omega}}{\sqrt{\widetilde{\Omega}^2-\boldsymbol{q}^2}}\right]}. \tag{3}$$

In Figs. 1(a)–1(b), we plot the associated spectral function, $\mathrm{Im}[D(\boldsymbol{q},\Omega)]$, as a function of q, Ω for two different values of $\tilde{\lambda}$.

For $\tilde{\lambda}\ll 1$, we recover the picture of standard Landau damping—the mode remains sharply defined until it enters the continuum and decays by emitting particle-hole pairs, resulting in a broadened dispersive mode [Fig. 1(a)]. There is a tiny expelled fraction outside the continuum, but the gap between the expelled fraction and the onset of continuum $\sim\tilde{\lambda}^2/2q^3$ [9], which makes it difficult to discern at large q. On the other hand, for $\tilde{\lambda}\gg 1$, part of the collective mode is repelled outside of the continuum [Fig. 1(b)], grazing along its edge; the remaining fraction enters the continuum and is damped strongly due to the larger coupling. Thus while it is impossible to avoid decay altogether, an appreciable fraction of the collective mode appears to escape the inevitable damping: this is what we refer to as interaction-mitigated Landau damping.

Note that the model by construction does not have any information associated with momentum transfer near $2k_F$, as shown in Figs. 1(a)–1(b). Next we address two questions, namely (i) what is the maximum spectral weight contained in the undamped branch of the collective mode in the asymptotic limit of $\tilde{\lambda}\gg 1$, and, (ii) is there a strong-coupling limit where the above picture can be applied using a controlled computation. We consider the quasiparticle residue associated with the collective mode, $Z_\Phi(\boldsymbol{q})=[1+\partial_{\Omega^2}\Pi_c'(\boldsymbol{q},\Omega)]^{-1}$, given by

$$Z_\Phi(\boldsymbol{q})=\left[1+\tilde{\lambda}\frac{\boldsymbol{q}^2}{2\tilde{\Omega}_{\mathrm{peak}}\left(\tilde{\Omega}_{\mathrm{peak}}^2-\boldsymbol{q}^2\right)^{3/2}}\right]^{-1}, \tag{4}$$

where Ω_{peak} denotes the renormalized dispersion for the long-lived collective mode outside the continuum, obtained as the solution to $D^{-1}(\boldsymbol{q},\Omega_{\mathrm{peak}})=0$. The numerical solution [9] for $Z_\Phi(\boldsymbol{q})$ for two different $\boldsymbol{q}$ values [dashed colored lines in Fig. 1(b)] is shown in Fig. 1(c) as a function of $\tilde{\lambda}$. Clearly, there are qualitative differences in the $\tilde{\lambda}$ dependence of $Z_\Phi(\boldsymbol{q})$ even for the collective mode branch lying outside the ph continuum, depending on whether for the specific $\boldsymbol{q}$ decay to particle-hole excitations is kinematically allowed.

Let us denote the crossing point between the collective mode and the onset of the continuum in the absence of a coupling ($\lambda=0$) as q_* [see Fig. 1(a)]. For the collective mode branch with $q<q_*$, Z_Φ decreases monotonically from $Z_\Phi(\lambda=0)=1$ with increasing $\tilde{\lambda}$; see the orange curve in Fig. 1(c). On the other hand, for the portion of the branch with $q>q_\star$, we find that Z_Φ increases monotonically from $Z_\Phi(\lambda=0)=0$ with increasing $\tilde{\lambda}$. After all, the branch does not exist outside the continuum at infinitesimal coupling, but develops a finite Z_Φ once it is pushed outside it. We find that for $\tilde{\lambda}\gg 1$, the spectral weight converges to $Z_\Phi(\boldsymbol{q})\to 1/2$ for both branches, suggesting a universal limit. The analytical expressions in the two limits is obtained as follows [9]: (i) for $\tilde{\lambda}\gg 1$, start from $Z_\Phi(\boldsymbol{q})=1/2$ and include the higher-order corrections in powers of $\delta q/\tilde{\lambda}$, where $\delta q=(2/q^2)|q_\star^2-q^2|^2$, and (ii) for $\tilde{\lambda}\ll 1$ and $q<q_\star$, $Z_\Phi(\boldsymbol{q})$ is computed in the limit $q\ll\widetilde{\Delta}$, whereas for $q>q_\star$ it is computed in the limit $q\gg\widetilde{\Delta}$, respectively. Explicitly,

$$Z_\Phi(q<q_\star)\simeq\begin{cases}1-\frac{|\boldsymbol{q}|^2}{2\widetilde{\Delta}^4}\tilde{\lambda}, & \tilde{\lambda}\ll 1,\\ \frac{1}{2}+\frac{3}{8}\left(\frac{\delta q}{\tilde{\lambda}}\right)^{1/2}, & \tilde{\lambda}\gg 1,\end{cases} \tag{5a}$$

$$Z_\Phi(q>q_\star)\simeq\begin{cases}\frac{2\tilde{\lambda}^2}{|\boldsymbol{q}|^4}, & \tilde{\lambda}\ll 1,\\ \frac{1}{2}-\frac{3}{8}\left(\frac{\delta q}{\tilde{\lambda}}\right)^{1/2}, & \tilde{\lambda}\gg 1.\end{cases} \tag{5b}$$

Note that even when $\lambda \ll 1$, a nonzero fraction of the spectral weight is contained in the branch of the collective mode that is repulsed outside the continuum. However, since both Z_Φ and the energy separation between the collective mode and the continuum are relative small ($\sim\tilde{\lambda}^2$), we focus on the strong coupling case for a clearer illustration of the effect.

Exact results for random flavor models. Given that our results are obtained in an RPA theory without a small parameter, we now turn to a solvable model where the analogous computations can be carried out in a controlled setting [10]. We reprise Eq. (1) and replicate the actions S_c, S_Φ to include N copies of fermions, $c^\dagger_{k,i}$, $c_{k,i}$ $(i = 1, \ldots, N)$ and M copies of the gapped collective mode, $\Phi_{q,\alpha}$ $(\alpha = 1, .., M)$. We replace the uniform Yukawa interaction, $S_{\rm int}$, by the random-flavor form [11–20],

$$S_{\rm int} \to \sqrt{\frac{2}{MN}} \sum_{i,i'} \sum_{\alpha} \sum_{r} \lambda_{i,i',\alpha} \Phi_{r,\alpha} c^\dagger_{r,i} c_{r,i'}. \tag{6}$$

Here the couplings $\lambda_{i,i',\alpha}$ are drawn from a random distribution with $\overline{\lambda_{i,i',\alpha}} = 0$ and $\overline{\lambda^2_{i,i',\alpha}} = \lambda^2$. We are interested in the large-N, M limit at fixed N/M. The RPA equations for the boson and fermion self-energy are exact in this limit for arbitrarily large λ [9]. While much of the recent interest in this model is tied to its non-Fermi-liquid regime, where the boson is critical, here we focus on the situation where the renormalized boson mass is fixed to be $\Delta^* = v_c$, with v_c the bare Fermi velocity. The metallic system remains in a renormalized Fermi liquid regime at low energies whenever Δ^* is finite.

Repeating the earlier analysis, we find that a significant spectral weight associated with the bosonic collective mode is repelled outside and continues to graze the edge of the renormalized ph continuum; see Figs. 1(d)–1(e). However, with increasing λ the mode appears to be broader (i.e., has a larger decay rate). The enhanced broadening is due to multiparticle decay, as shown by the Feynman diagram in Fig. 1(f). Note that such processes are automatically included in the self-consistent equations for the boson lifetime, leading to $\Sigma''_\Phi(\Omega) \sim \tilde{\lambda}^3\Omega$ at $q = 0$ [9].

Our computations thus highlight the nontrivial aspects associated with both decay into, and level repulsion from, a multiparticle continuum in a renormalized Fermi liquid for arbitrarily strong interactions. While it is rare to find realistic model Hamiltonians where theoretically well-controlled computations can be carried out in the strong-coupling limit, we find that RPA already captures much of the essence of the underlying physics.

We next turn to the charge response in graphene, and moiré graphene, in the presence of screened Coulomb interactions. Importantly, instead of focusing on an independent bosonic mode, we focus on the intrinsic plasmon excitation and analyze the regime where it is repelled from the continuum.

Charge response in graphenelike models. We will begin by analyzing numerically the charge response for the usual honeycomb model of graphene, with the Coulomb interaction treated at the RPA level. The ph continuum in graphene is well known to host an intra- and interband contribution: $\Pi(\boldsymbol{q}, \Omega) = 2[\Pi_{\rm intra}(\boldsymbol{q}, \Omega) + \Pi_{\rm inter}(\boldsymbol{q}, \Omega)]$, where the factor of 2 is due to spin degeneracy. The full RPA charge susceptibility is

$$\chi(\boldsymbol{q}, \Omega) = \frac{\Pi(\boldsymbol{q}, \Omega)}{1 - V(\boldsymbol{q})\Pi(\boldsymbol{q}, \Omega)}. \tag{7}$$

We allow ourselves the freedom to tune the strength of Coulomb interaction, $V(\boldsymbol{q})$, by effectively varying the charge of the electron. We will demonstrate that for strong enough Coulomb interaction and heavy doping, the plasmon mode is completely pushed out of the intraband continuum, enters partially inside the interband continuum at a momentum $q_\star$, and is repelled partially away from the interband continuum; see Figs. 2(a)–2(b). For a two-dimensional (2D) Coulomb interaction derived from an underlying one in three dimensions, $V(\boldsymbol{q}) = 2\pi e^2/\kappa q$, where κ is an effective dielectric constant. To compare the scale of the Coulomb interaction with the graphene bare bandwidth, W_0, we define a dimensionless Coulomb potential [9], $\tilde{V}(\boldsymbol{q}) = 2\pi e^2/(\kappa a_0^2 W_0 q) = \tilde{e}^2/a_0 q$. The dimensionless interaction strength $\tilde{e}^2 \equiv 2\pi e^2/\kappa a_0 W_0$ (a_0 is the lattice constant). We are now in a position to obtain an analytical understanding of the level repulsion in graphene, building on the results of our earlier simple models.

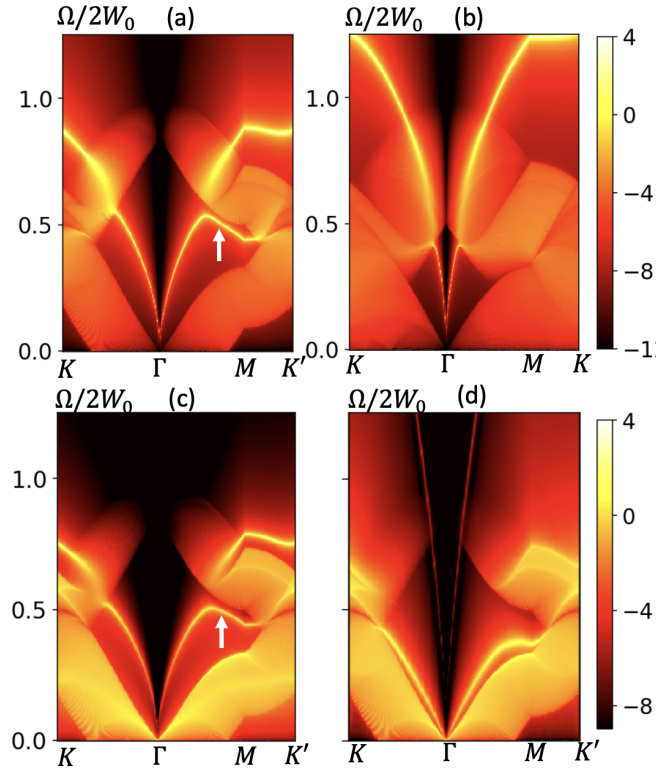

FIG. 2. Numerical results for the spectral function, $\log \mathrm{Im}[\chi(q, \Omega)]$, for graphene [without substrate in (a), (b)] with 2D Coulomb interaction with $\tilde{e}^2 = 15 \simeq 6\tilde{e}^2_{\rm real}$. The Fermi energies are (a) $E_F/W_0 \simeq 0.83$ (b) $E_F/W_0 \simeq 0.5$, respectively, where E_F is measured relative to charge neutrality. The plasmon is repelled from the interband continuum, and its dispersion develops a negative slope in the region indicated by the white arrows. Numerical results for $\log \mathrm{Im}[\chi(q, \Omega)]$ for graphene on a metallic substrate (without direct electron tunneling) coupled through Coulomb interaction with $\tilde{e}^2 = 7$ for (c) $v_F^{\rm sub} < v_F^{\rm G}$, and (d) $v_F^{\rm sub} > v_F^{\rm G}$. The red line with the largest slope is the plasmon mode of the substrate.

Within RPA and for $q \to 0$ and $(2E_F - \Omega - v_F q) \to 0$, the asymptotic expressions [21–24] for $\Pi_{\text{intra}}(\boldsymbol{q}, \Omega)$ and $\Pi_{\text{inter}}(\boldsymbol{q}, \Omega)$ are given by [9]

$$\Pi_{\text{intra}}(\boldsymbol{q}, \Omega) = \left[1 - \frac{\tilde{\Omega}}{\sqrt{\tilde{\Omega}^2 - |\boldsymbol{q}|^2}}\right], \tag{8a}$$

$$\Pi_{\text{inter}}(\boldsymbol{q}, \Omega) \simeq \pi[(\tilde{\Omega} - 2\tilde{E}_F) + \sqrt{(\tilde{\Omega} - 2\tilde{E}_F)^2 - |\boldsymbol{q}|^2}] + \Pi_{\text{reg}} \tag{8b}$$

where $\tilde{\Omega} \equiv \Omega/v_F$, $\tilde{E}_F \equiv E_F/v_F$, and Π_{reg} includes additional nonsingular terms. The pole structure of Eq. (7) in the limit $\Omega \gg |\boldsymbol{q}|$ is given by,

$$\chi(\boldsymbol{q}, \Omega) \approx \frac{\Pi(\boldsymbol{q}, \Omega)}{1 - \frac{\beta_0|\boldsymbol{q}|}{\tilde{\Omega}^2} - \frac{\tilde{e}^2}{|\boldsymbol{q}|}\Pi_{\text{inter}}(\boldsymbol{q}, \Omega)}. \tag{9}$$

The $1 - (\beta_0|\boldsymbol{q}|/\tilde{\Omega}^2)$ term is obtained upon expanding $V(\boldsymbol{q})\Pi_{\text{intra}}(q, \Omega)$ in powers of $|\boldsymbol{q}|/\tilde{\Omega}$, leading to a plasmon mode with dispersion $\Omega \sim \sqrt{\beta_0|\boldsymbol{q}|}$ ($\beta_0 = \pi e^2/\kappa W_0$), which is coupled to the interband continuum through the Coulomb interaction. Solving for $\text{Re}\chi^{-1}(\boldsymbol{q}, \Omega) = 0$ yields the dispersion of the mode that avoids repulsion from the interband continuum, in a manner analogous to our earlier discussion.

To study the consequences of dynamical screening of the Coulomb interaction on the phenomenology of level repulsion, we have also analyzed the charge response in a bilayer system where a single sheet of graphene (with a Fermi velocity denoted v_F^{G}) is coupled via Coulomb interaction to a metallic Fermi liquid substrate. We describe the latter microscopically by a lattice model of electrons on a triangular lattice with Fermi velocity, v_F^{sub}. We choose the filling such that $E_F^{\text{sub}} = 0.6W_0^{\text{sub}}$, where W_0^{sub} is the electronic bandwidth in the substrate. Note that we exclude direct hopping of electrons between the two layers, such that there is a $U(1) \times U(1)$ symmetry associated with the two conserved densities. Within RPA, the dynamics of both charge degrees of freedom is coupled in a nontrivial fashion. For $v_F^{\text{sub}} < v_F^{\text{G}}$ [Fig. 2(c)], the phenomenology of level repulsion is qualitatively similar to where the substrate is absent [Fig. 2(a)], and the latter only modifies the results quantitatively by screening the Coulomb potential. Importantly, in this case, the onset of the ph continuum for the substrate lies inside the graphene ph continuum. On the other hand, for $v_F^{\text{sub}} > v_F^{\text{G}}$ [Fig. 2(d)], the graphene plasmon decays into the ph continuum of the metallic substrate before entering the graphene interband continuum. As a result the phenomenology changes qualitatively. This illustrates that, in principle, the fate of the graphene plasmon can be determined by tuning the properties (e.g., density, bandwidth) associated with an underlying substrate in a controllable device geometry.

Charge response in twisted bilayer graphenelike models. Our results so far suggest that heavily doped graphene ($E_F/W_0 \sim 0.8$, where W_0 is the bandwidth) with larger than usual strength of Coulomb interaction can display an avoided level repulsion of the plasmon from the interband continuum. Let us now turn to the related setup of twisted bilayer graphene, in order to analyze the extent of possible phenomenological similarities. We focus on angles away from magic angle, where the isolated bands are not flat and the effects of Coulomb interactions can be justifiably treated within RPA.

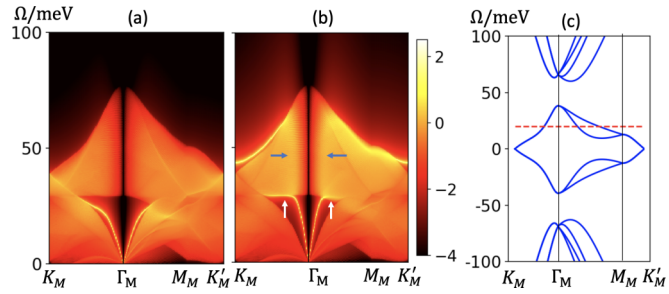

FIG. 3. Numerical results for the dielectric function [Eq. (10)], $\log \text{Im}[\varepsilon^{-1}(q, \Omega)_{G=0}]$, for the model with interactions projected to flat bands, for twisted bilayer graphene at $\theta = 1.4$ for (a) realistic parameters, and (b) enhanced Coulomb interaction (see main text). The level repulsion associated with the plasmon is marked by white arrows. (c) Band structure at $\theta = 1.4$, with dashed line denoting the chemical potential $E_F = 20$ meV.

We begin with the Bistritzer-Macdonald (BM) model [25–28] at twist angle $\theta = 1.4$, and include the effect of a screened Coulomb interaction, $V(\boldsymbol{q}) = (2\pi e^2/\kappa q)\tanh(\xi q)$, where the background dielectric constant $\kappa \simeq 6$ with a screening length $\xi \simeq 10$ nm [9]. The numerical results for the charge response are shown in Fig. 3, where we plot the dielectric function [9,29,30] to leading order, after projecting to the flat bands,

$$\varepsilon_{\boldsymbol{G}}^{-1}(\boldsymbol{q}, \Omega) = \left[1 - \sum_{\eta} V(\boldsymbol{q} + \boldsymbol{G})\Pi_{\boldsymbol{G}}^{\eta}(\boldsymbol{q}, \Omega)\right]^{-1}, \tag{10}$$

with η denoting the valley index and $\boldsymbol{G}$ the reciprocal lattice vector in the moiré Brillouin zone. Interestingly, the experimentally realistic value of Coulomb interaction does not immediately repel the plasmon from the continuum [Fig. 3(a)], as was the case for single-layer graphene. However, if the strength of Coulomb interaction is increased (by a factor of 4), a clear signature appears of plasmon level repulsion from the interband continuum [Fig. 3(b)] for the density shown in Fig. 3(c). A fraction of the plasmon is repelled outside the interband ph continuum near q_* (marked by white arrows), while the rest enters the continuum (marked by blue arrows) and is Landau damped. For $\Omega \gtrsim 70$ meV, the plasmon exits the interband ph continuum and remains undamped. Although the plasmon above the interband ph continuum may finally decay into the continuum associated with the remote bands, the fraction of plasmon repelled below the interband continuum remains undamped [9]. While the latter mechanism was studied in previous work [21], our observations point out a distinct mechanism to avoid plasmon decay via level repulsion from the continuum. As long as the interaction between the plasmon and the interband continuum is kinematically allowed (e.g., achieved by increasing the strength of the effective Coulomb interaction), the mechanism of level repulsion discussed here can appear in tandem with the unrelated mechanism pointed out in previous work [21] at different energy scales.

Outlook. A number of experiments have reported measurements of the plasmon mode at room temperature using

terrahertz near-field microscopy in graphene-based structures, ranging from microribbon [31], single layer [32–35], to even twisted bilayer graphene away from magic angle [36]. These experiments have focused primarily on the low-doping regime [32–35], or at high energies (∼200 meV) where the interband plasmon lies between the flat and remote bands [36,37], respectively. These relatively high-temperature measurements also have inevitable thermal broadening (∼25 meV), which makes it challenging to resolve a broadened plasmon that is repelled outside the continuum. However, with further technical advances in optical microscopy and identification of the ideal dielectric environment, future experiments will hopefully be able to observe an avoided level repulsion and an undamped plasmon.

On the theoretical front, a numerically exact investigation of the coupled dynamics of an intrinsic collective mode and the many-particle continuum in electronic models beyond an RPA-like expansion, used very commonly also in other settings related to ours [38], is clearly desirable. A possible path would be to investigate correlated one-dimensional lattice models using time-dependent density matrix renormalization group techniques. Finally, whether a possible generalization of the same mechanism for avoiding (partially) a decay of the collective mode in non-Fermi-liquid metals without long-lived quasiparticles [39–41] exists, remains an interesting open question.

Acknowledgments. We thank K. Schalm and J. Zaanen for discussions, and especially A. Chubukov and C. Lewandowski for a number of useful suggestions based on a critical reading of an earlier version of this manuscript. X.W. thanks J. F. Méndez-Valderrama for a number of useful suggestions related to the numerical simulations. D.C. acknowledges the hospitality of the Max Planck Institute for the Physics of Complex Systems during the final stages of this work. This work is supported in part by a CAREER grant from the NSF to D.C. (DMR-2237522) and by the Deutsche Forschungsgemeinschaft under grant cluster of excellence ct.qmat (EXC 2147, project id 390858490).

[1] A. A. Abrikosov, I. Dzyaloshinskii, L. P. Gorkov, and R. A. Silverman, *Methods of Quantum Field Theory in Statistical Physics* (Dover, New York, 1975).

[2] D. Pines and P. Nozières, *Theory of Quantum Liquids: Normal Fermi Liquids* (CRC Press, Boca Raton, 2018).

[3] D. N. Basov, M. M. Fogler, and F. J. G. de Abajo, Polaritons in van der Waals materials, Science **354**, aag1992 (2016).

[4] G. X. Ni, A. S. McLeod, Z. Sun, L. Wang, L. Xiong, K. W. Post, S. S. Sunku, B.-Y. Jiang, J. Hone, C. R. Dean, M. M. Fogler, and D. N. Basov, Fundamental limits to graphene plasmonics, Nature (London) **557**, 530 (2018).

[5] M. E. Zhitomirsky, Decay of quasiparticles in quantum spin liquids, Phys. Rev. B **73**, 100404(R) (2006).

[6] R. N. Bhatt and W. L. McMillan, Theory of anomalous dispersion in liquid He^4, Phys. Rev. A **10**, 1591 (1974).

[7] R. Verresen, R. Moessner, and F. Pollmann, Avoided quasiparticle decay from strong quantum interactions, Nat. Phys. **15**, 750 (2019).

[8] B. Gaveau and L. S. Schulman, Limited quantum decay, J. Phys. A: Math. Gen. **28**, 7359 (1995).

[9] See Supplemental Material at http://link.aps.org/supplemental/10.1103/PhysRevB.109.L121102 for additional details on the theoretical and numerical computations, which includes Refs. [42–45].

[10] D. Chowdhury, A. Georges, O. Parcollet, and S. Sachdev, Sachdev-Ye-Kitaev models and beyond: Window into non-fermi liquids, Rev. Mod. Phys. **94**, 035004 (2022).

[11] H. Guo, A. A. Patel, I. Esterlis, and S. Sachdev, Large-*n* theory of critical Fermi surfaces. II. Conductivity, Phys. Rev. B **106**, 115151 (2022).

[12] W. Fu, D. Gaiotto, J. Maldacena, and S. Sachdev, Supersymmetric Sachdev-Ye-Kitaev models, Phys. Rev. D **95**, 026009 (2017).

[13] A. A. Patel and S. Sachdev, Critical strange metal from fluctuating gauge fields in a solvable random model, Phys. Rev. B **98**, 125134 (2018).

[14] E. Marcus and S. Vandoren, A new class of SYK-like models with maximal chaos, J. High Energy Phys. 01 (2019) 166.

[15] Y. Wang, Solvable strong-coupling quantum dot model with a non-Fermi-liquid pairing transition, Phys. Rev. Lett. **124**, 017002 (2020).

[16] I. Esterlis and J. Schmalian, Cooper pairing of incoherent electrons: An electron-phonon version of the Sachdev-Ye-Kitaev model, Phys. Rev. B **100**, 115132 (2019).

[17] Y. Wang and A. V. Chubukov, Quantum phase transition in the Yukawa-SYK model, Phys. Rev. Res. **2**, 033084 (2020).

[18] J. Kim, E. Altman, and X. Cao, Dirac fast scramblers, Phys. Rev. B **103**, L081113 (2021).

[19] E. E. Aldape, T. Cookmeyer, A. A. Patel, and E. Altman, Solvable theory of a strange metal at the breakdown of a heavy Fermi liquid, Phys. Rev. B **105**, 235111 (2022).

[20] W. Wang, A. Davis, G. Pan, Y. Wang, and Z. Y. Meng, Phase diagram of the spin-1/2 Yukawa-Sachdev-Ye-Kitaev model: Non-Fermi liquid, insulator, and superconductor, Phys. Rev. B **103**, 195108 (2021).

[21] C. Lewandowski and L. Levitov, Intrinsically undamped plasmon modes in narrow electron bands, Proc. Natl. Acad. Sci. USA **116**, 20869 (2019).

[22] S. Das Sarma, S. Adam, E. H. Hwang, and E. Rossi, Electronic transport in two-dimensional graphene, Rev. Mod. Phys. **83**, 407 (2011).

[23] E. H. Hwang and S. Das Sarma, Dielectric function, screening, and plasmons in two-dimensional graphene, Phys. Rev. B **75**, 205418 (2007).

[24] B. Wunsch, T. Stauber, F. Sols, and F. Guinea, Dynamical polarization of graphene at finite doping, New J. Phys. **8**, 318 (2006).

[25] R. Bistritzer and A. H. MacDonald, Moiré bands in twisted double-layer graphene, Proc. Natl. Acad. Sci. USA **108**, 12233 (2011).

[26] M. Koshino, N. F. Q. Yuan, T. Koretsune, M. Ochi, K. Kuroki, and L. Fu, Maximally localized Wannier orbitals and the

extended Hubbard model for twisted bilayer graphene, Phys. Rev. X **8**, 031087 (2018).

[27] B. A. Bernevig, Z.-D. Song, N. Regnault, and B. Lian, Twisted bilayer graphene. I. Matrix elements, approximations, perturbation theory, and a $k \cdot p$ two-band model, Phys. Rev. B **103**, 205411 (2021).

[28] B. A. Bernevig, Z.-D. Song, N. Regnault, and B. Lian, Twisted bilayer graphene. III. Interacting Hamiltonian and exact symmetries, Phys. Rev. B **103**, 205413 (2021).

[29] N. Wiser, Dielectric constant with local field effects included, Phys. Rev. **129**, 62 (1963).

[30] S. L. Adler, Quantum theory of the dielectric constant in real solids, Phys. Rev. **126**, 413 (1962).

[31] L. Ju, B. Geng, J. Horng, C. Girit, M. Martin, Z. Hao, H. A. Bechtel, X. Liang, A. Zettl, Y. R. Shen, and F. Wang, Graphene plasmonics for tunable terahertz metamaterials, Nat. Nanotech. **6**, 630 (2011).

[32] D. B. Ruiz, N. C. H. Hesp, H. H. Sheinfux, C. R. Marimón, C. M. Maissen, A. Principi, R. Asgari, T. Taniguchi, K. Watanabe, M. Polini, R. Hillenbrand, I. Torre, and F. H. L. Koppens, Experimental signatures of the transition from acoustic plasmon to electronic sound in graphene, Sci. Advan. **9**, eadi0415 (2023).

[33] P. Alonso-González, A. Y. Nikitin, Y. Gao, A. Woessner, M. B. Lundeberg, A. Principi, N. Forcellini, W. Yan, S. Vélez, A. J. Huber, K. Watanabe, T. Taniguchi, F. Casanova, L. E. Hueso, M. Polini, J. Hone, F. H. L. Koppens, and R. Hillenbrand, Acoustic terahertz graphene plasmons revealed by photocurrent nanoscopy, Nat. Nanotech. **12**, 31 (2017).

[34] Z. Fei, A. S. Rodin, G. O. Andreev, W. Bao, A. S. McLeod, M. Wagner, L. M. Zhang, Z. Zhao, M. Thiemens, G. Dominguez, M. M. Fogler, A. H. C. Neto, C. N. Lau, F. Keilmann, and D. N. Basov, Gate-tuning of graphene plasmons revealed by infrared nano-imaging, Nature (London) **487**, 82 (2012).

[35] L. Jiang, Z. Shi, B. Zeng, S. Wang, J.-H. Kang, T. Joshi, C. Jin, L. Ju, J. Kim, T. Lyu, Y.-R. Shen, M. Crommie, H.-J. Gao, and F. Wang, Soliton-dependent plasmon reflection at bilayer graphene domain walls, Nat. Mater. **15**, 840 (2016).

[36] N. C. H. Hesp, I. Torre, D. Rodan-Legrain, P. Novelli, Y. Cao, S. Carr, S. Fang, P. Stepanov, D. Barcons-Ruiz, H. Herzig Sheinfux, K. Watanabe, T. Taniguchi, D. K. Efetov, E. Kaxiras, P. Jarillo-Herrero, M. Polini, and F. H. L. Koppens, Observation of interband collective excitations in twisted bilayer graphene, Nat. Phys. **17**, 1162 (2021).

[37] S. S. Sunku, A. S. McLeod, T. Stauber, H. Yoo, D. Halbertal, G. Ni, A. Sternbach, B.-Y. Jiang, T. Taniguchi, K. Watanabe, P. Kim, M. M. Fogler, and D. N. Basov, Nano-photocurrent mapping of local electronic structure in twisted bilayer graphene, Nano Lett. **20**, 2958 (2020).

[38] S. Maiti, J. Knolle, I. Eremin, and A. V. Chubukov, Effect of nodes, ellipticity, and impurities on the spin resonance in iron-based superconductors, Phys. Rev. B **84**, 144524 (2011).

[39] X. Wang and D. Chowdhury, Collective density fluctuations of strange metals with critical Fermi surfaces, Phys. Rev. B **107**, 125157 (2023).

[40] A. V. Chubukov, Ward identities for strongly coupled Eliashberg theories, Phys. Rev. B **72**, 085113 (2005).

[41] A. Romero-Bermúdez, A. Krikun, K. Schalm, and J. Zaanen, Anomalous attenuation of plasmons in strange metals and holography, Phys. Rev. B **99**, 235149 (2019).

[42] E. H. Hwang, R. Sensarma, and S. Das Sarma, Plasmon-phonon coupling in graphene, Phys. Rev. B **82**, 195406 (2010).

[43] T. Cea and F. Guinea, Coulomb interaction, phonons, and superconductivity in twisted bilayer graphene, Proc. Natl. Acad. Sci. USA **118**, e2107874118 (2021).

[44] A. Fahimniya, C. Lewandowski, and L. Levitov, arXiv:2011.02982.

[45] M. Papaj and C. Lewandowski, Probing correlated states with plasmons, Sci. Adv. **9**, eadg3262 (2023).